Schweizerischer Erdbebendienst
Service Sismologique Suisse
Servizio Sismico Svizzero
Swiss Seismological Service

ETH
Eidgenössische Technische Hochschule Zürich
Swiss Federal Institute of Technology Zurich

SITE CHARACTERIZATION REPORT

SAARA: Aarau (AG)

Francesco Panzera, Manuel Hobiger, Donat Fäh

Last Modification: 15th November, 2019

Schweizerischer Erdbebendienst (SED)
Service Sismologique Suisse
Servizio Sismico Svizzero
Servizi da Terratrembels Svizzer
ETH Zürich
Sonneggstrasse 5
8092 Zürich
Schweiz
francesco.panzera@sed.ethz.ch

Contents

Summary

Aarau (AG), located in northern Switzerland, was selected as site for the installation of a new station, called SAARA, as part of the renewal project of the Swiss Strong Motion Network (SSMNet). In order to better assess the local underground, we performed site characterization measurements with different techniques. The results of the horizontal-to-vertical spectral ratio (H/V), show curves with clear peaks between 8.0 and 16.0 Hz. The variability in the frequency peak is related to a dipping of the bedrock towards south underneath the station.

The inversion of the passive seismic array measurements allows us to infer a main possible discontinuity above the bedrock at about 5-6 m. The bedrock has a velocity of about 1600 m/s, whereas the shear-wave velocity above is about 250 m/s. The V_{S30} value of the site is about 766 m/s, corresponding to soil class B in EC8 and E in SIA261.

The theoretical shear-wave transfer functions predict an amplification peak at about 10.0 Hz, in quite good agreement with the fundamental H/V frequency of the site where the strong motion station is installed.

1 Introduction

The station SAARA is part of the Swiss Strong Motion Network (SSMNet). The station has been installed on 7 August 2018 in the framework of the second phase of the Swiss Strong Motion Network (SSMNet) renewal project (Fig. 1). In order to better characterize the underground of the station, we performed passive array measurements.
The site is of interest because it is located in a populated area in central Switzerland on the Molasse basin.
The measurement campaign was carried out on 25 April 2019 in order to characterize the soil column in terms of fundamental frequency and shear wave velocity.

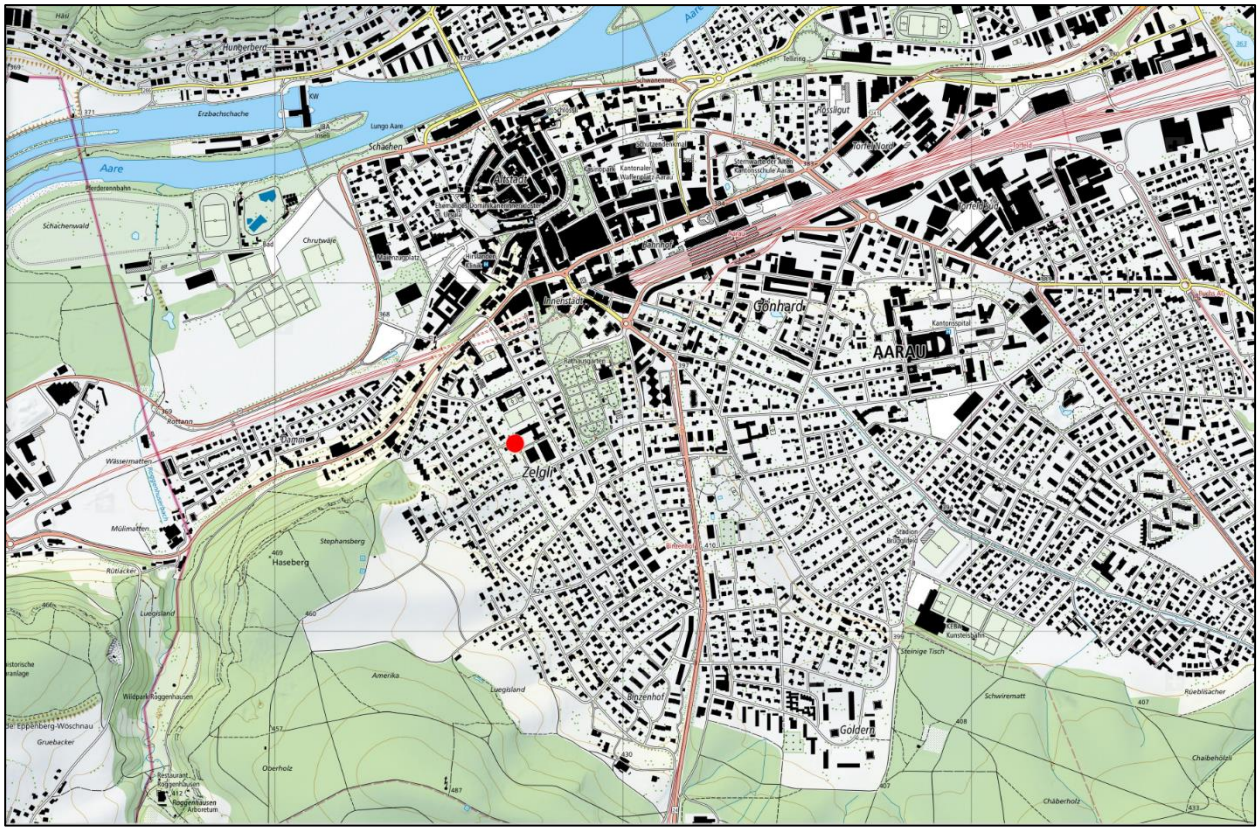

Figure 1: Map showing the location of the strong motion station (red circle) in Aarau. © 2019 swisstopo (JD100042)

2 Geological setting

A geological map of the surroundings of the site in Aarau is shown in Fig. 2, together with the stations of the passive array measurements. All 16 stations of the passive array measurement and station SAARA are located on a Löss deposit terrace.

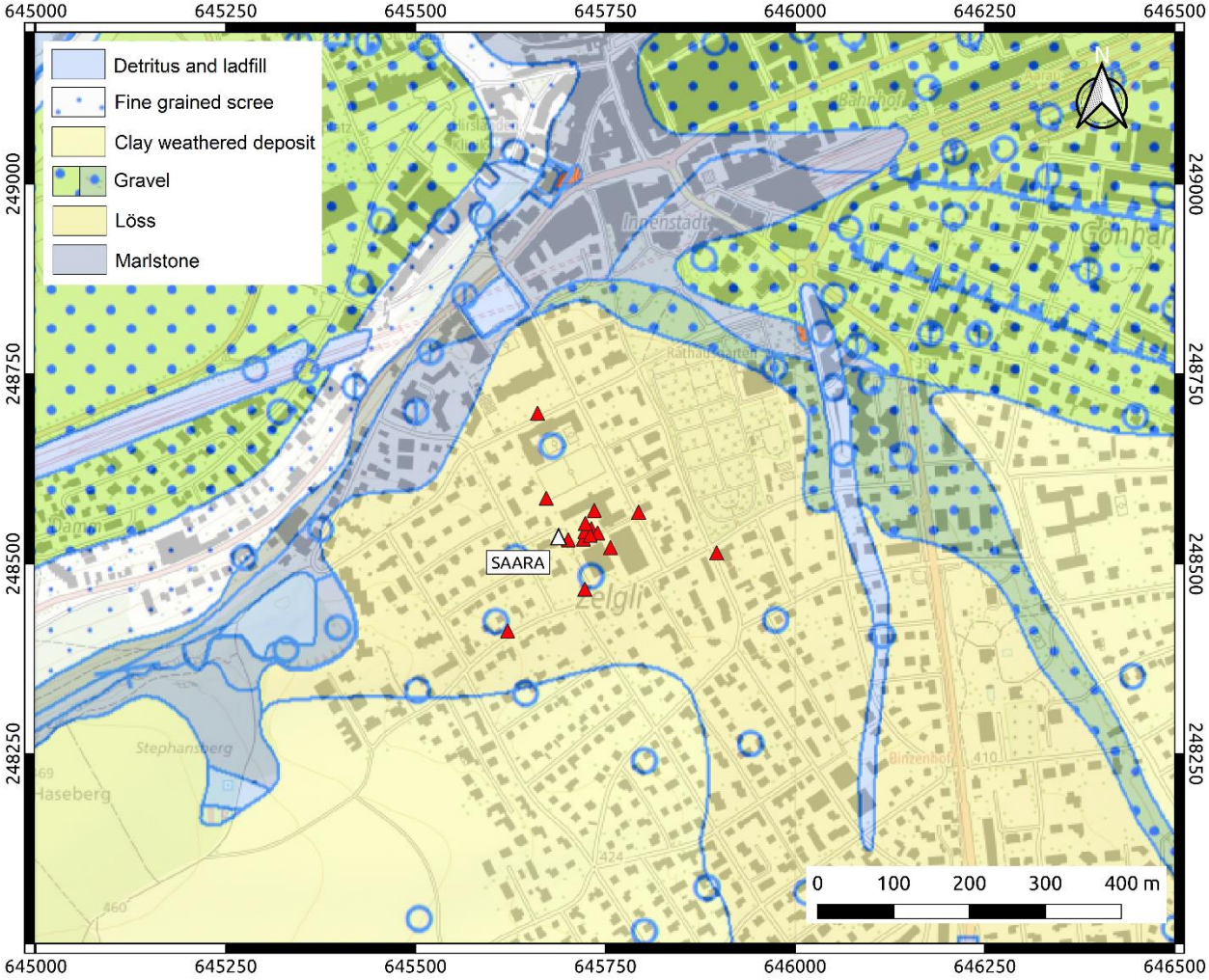

Figure 2: Geological map of the area around the seismic station SAARA. The stations of the passive array recordings are indicated by red triangles, whereas SAARA is indicated by a white triangle. © 2019 swisstopo (JD100042)

3 Site characterization measurements

3.1 Data set

To characterize the deeper underground structure around the seismic station, we performed passive seismic measurements in April 2019, together with an H/V measurement close to SAARA (Fig. 3).

A single array of 16 stations was installed (Fig. 4). The stations were planned to be located on five rings of different radii around a central station. The inner three rings were planned in regular forms with angular distances of 120° between the different stations on the ring. These three rings had radii of 5, 12 and 29 m, respectively. The second and third rings were rotated by 40° with respect to the first and second rings, respectively. These three rings were installed using a measuring tape and a plan of the intended orientations from the central station. The fourth ring was planned to have a distance of 72 m from the central station. The stations of the fifth ring were placed at distances of about 170 m from the array center. The minimum and maximum interstation distances in the finally installed array were 5.0 and 170 m, respectively.

Each station consisted of a Lennartz 5s sensor connected to a Centaur digitizer, where four stations in the central part had two sensors connected to the same digitizer. The station names of the array are composed of "SAA" followed by a three-digit number between 42 and 49, 52 and 55, 63, 65, 68 and 73 (corresponding to the Centaur digitizer serial number for numbers lower than 60 and serial number plus 20 for higher numbers). The array recording time was 150 minutes (9000 s). The station locations have been measured by a differential GPS system (Leica Viva GS10) which was set up to measure with a precision better than 5 cm.

Figure 3: Seismic station installation example for the measurements in Aarau.

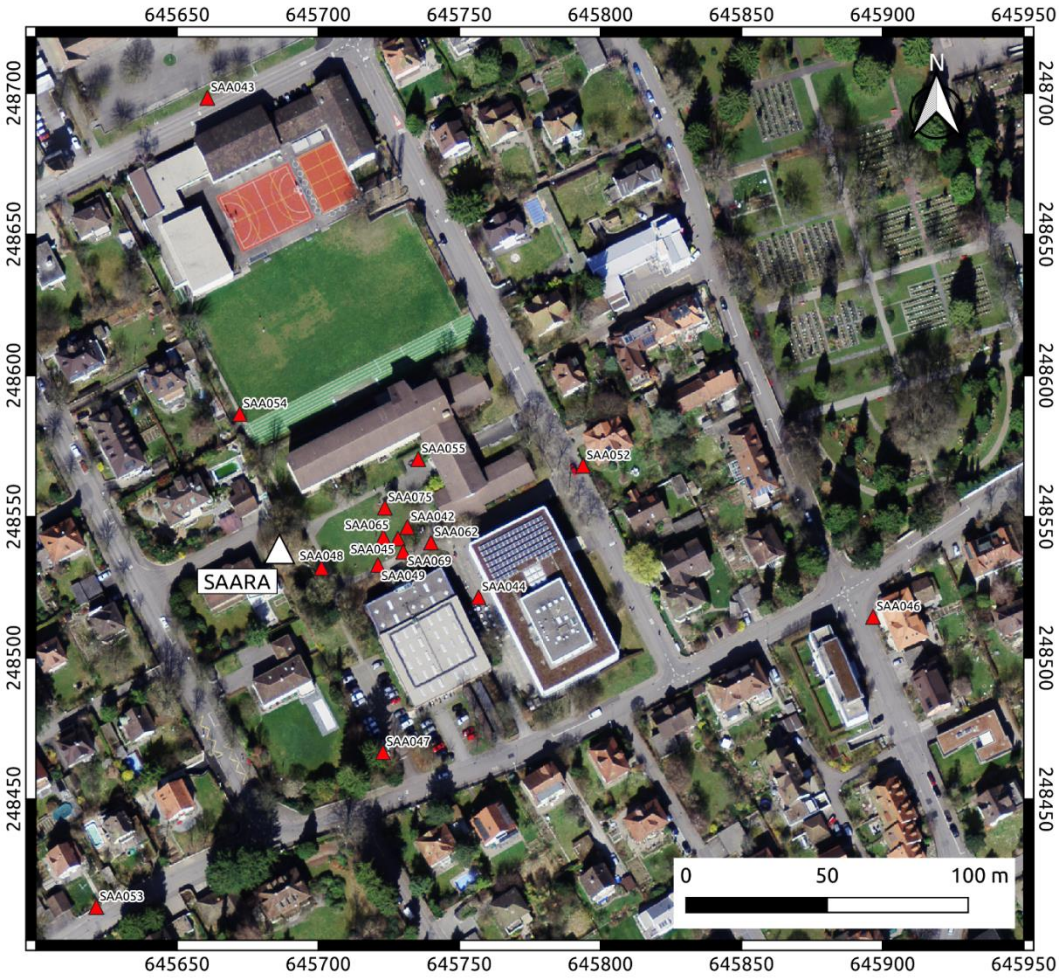

Figure 4: Layout of the array measurement in Aarau. The locations of the stations for the passive seismic measurement are indicated by red triangles. In particular, SAA048 was performed nearby the station site (15 m). © 2019 swisstopo (JD100042)

3.2 H/V and RayDec ellipticity curves

Figure 5 shows the H/V curves determined with the time-frequency analysis method (Fäh et al., 2009) for all stations of the passive array. The H/V curves are homogeneous and show a similar pattern up to 4.0 Hz, above this frequency value most of the curves are characterized by peaks between 10.0 and about 13.0 Hz. Only in five cases the fundamental frequency is outside this range. In particular, frequencies lower than 10.0 Hz are observed at the sites SAA046, SAA047 and SAA053, a peak at about 16.00 Hz is observed in the site SAA043. This behavior indicates a slight slope towards South of the Löss layer.
The RayDec technique (Hobiger et al., 2009) is meant to eliminate the contributions of other wave types than Rayleigh waves and give a better estimate of the ellipticity than the classical H/V technique. The RayDec ellipticity curves for all stations of the array measurement are shown in Figure 5. The RayDec curves of the different stations are also not homogeneous, but show different fundamental peaks.

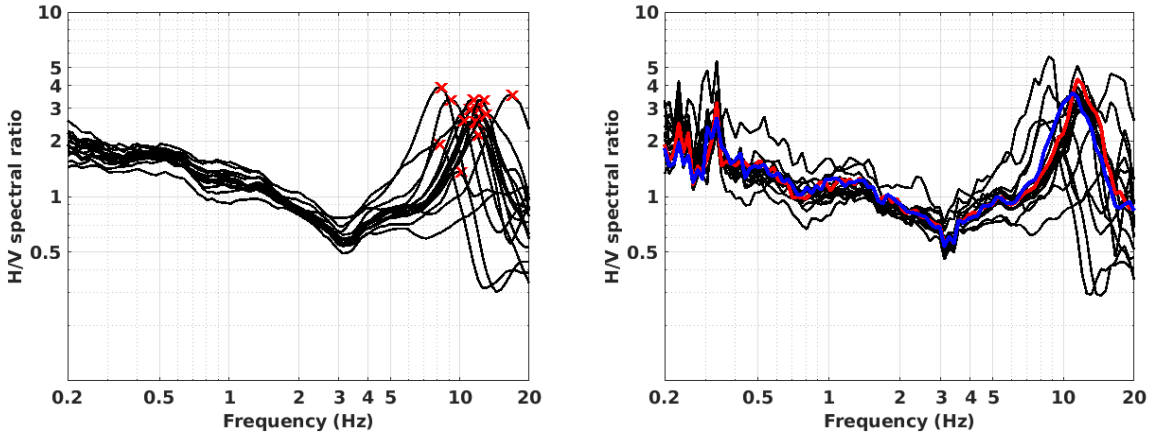

Figure 5: Left: H/V curves of the different stations of the array measurement in Aarau. Right: RayDec ellipticities for all stations of the array. The curve of SAA045, the array center is highlighted in red, whereas SAA048 measurement nearby the station is highlighted in blue.

3.3 Polarization measurements

The polarization analysis was performed according to Burjánek et al. (2010) and Burjánek et al. (2012). The results for all stations of the array are similar. Only the results for SAA045, the station in the array center, are shown in Fig. 6. The results show that the ground motion is almost linear and horizontally polarized around the H/V peak. In the polar plot, no pronounced polarization directions are present.

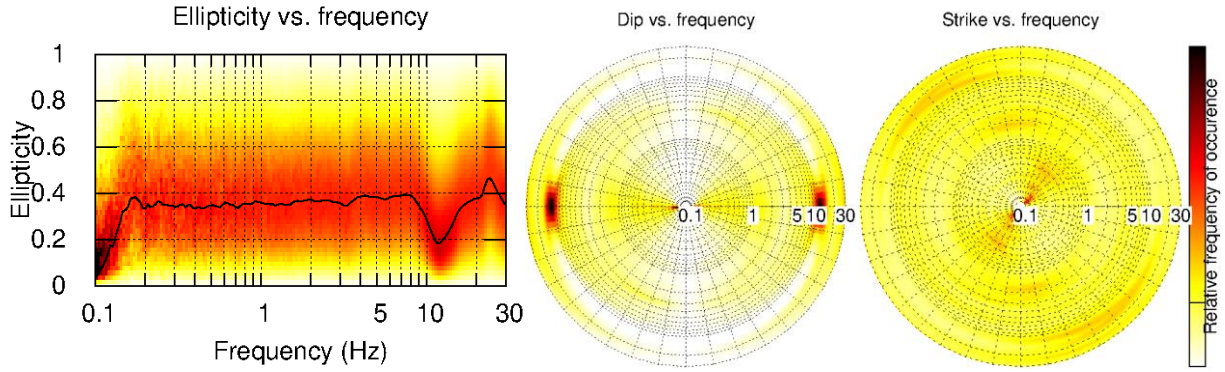

Figure 6: Polarization analysis of station SAA045.

3.4 3-component high-resolution FK

The results of the 3-component high-resolution FK analysis (Poggi and Fäh, 2010) are shown in Fig. 7. The result on the transverse component shows the dispersion curves (DC) of two modes of Love waves: the first one, from 4.0 to 6.0 Hz, is outside the array resolution limits; the second mode is picked from 6.9 to 16.8 Hz. On the radial component, one mode is visible in the frequency range 8.0 to 23.0 Hz. On the vertical component, one mode was picked from 3.4 to 10.5 Hz, whereas another one was picked above 11.6 Hz. The corresponding ellipticity curves of the radial and vertical components are clearly identified in the respective frequency range. In particular, the radial shows a peak at about 15.0 Hz, whereas the transverse one is almost flat.

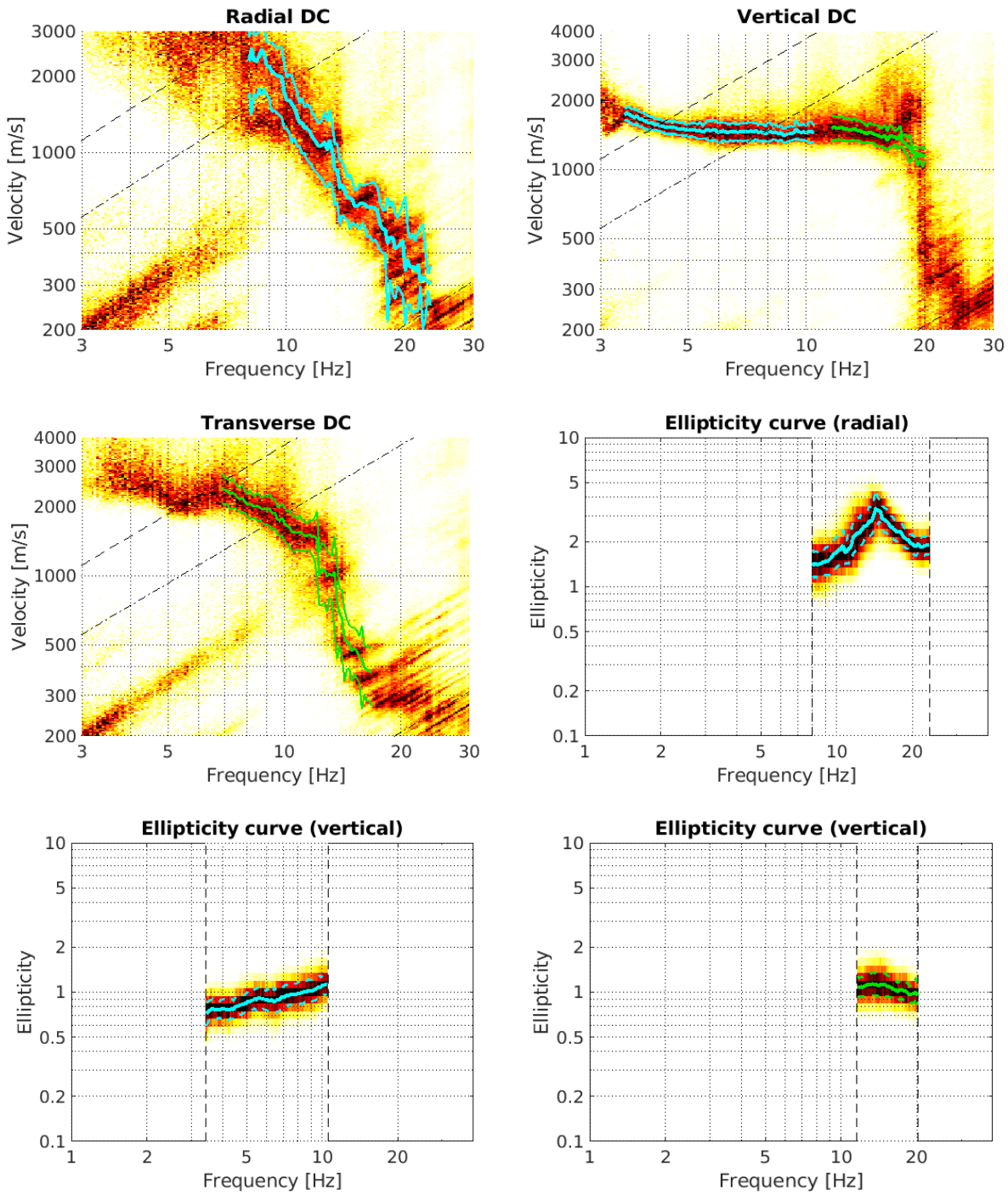

Figure 7: Dispersion and ellipticity curves for the transverse, radial and vertical components obtained with the 3-component HRFK algorithm (Poggi and Fäh, 2010). The dashed and dotted black lines are the array resolution limits. The solid cyan and green lines are picked from the data, where the central line indicates the best value and the two outer lines the standard deviation, respectively.

3.5 WaveDec

The results of the WaveDec (Maranò et al., 2012) processing are shown in Fig. 8. This technique estimates the properties of single or multiple waves simultaneously with a maximum likelihood approach. In order to get good results, the parameter γ has been tuned to modify the sharpness of the wave property estimation between purely maximum likelihood estimation and a Bayesian Information Criterion. Here, a value of $\gamma = 0.2$ was used, corresponding to a mostly maximum likelihood estimation.
The Love wave dispersion curve is clearly retrieved for one continuous mode between about 4.5 and 24.2 Hz. The Rayleigh wave dispersion curve can be picked between 4.5 Hz and 18.5 Hz. The ellipticity angle for the picked Rayleigh wave dispersion curve is negative for all the considered frequency range, indicating retrograde particle motion. The ellipticity angle goes towards -90° above 10 Hz, which would be compatible with a singular peak and a change of the particle motion to prograde.

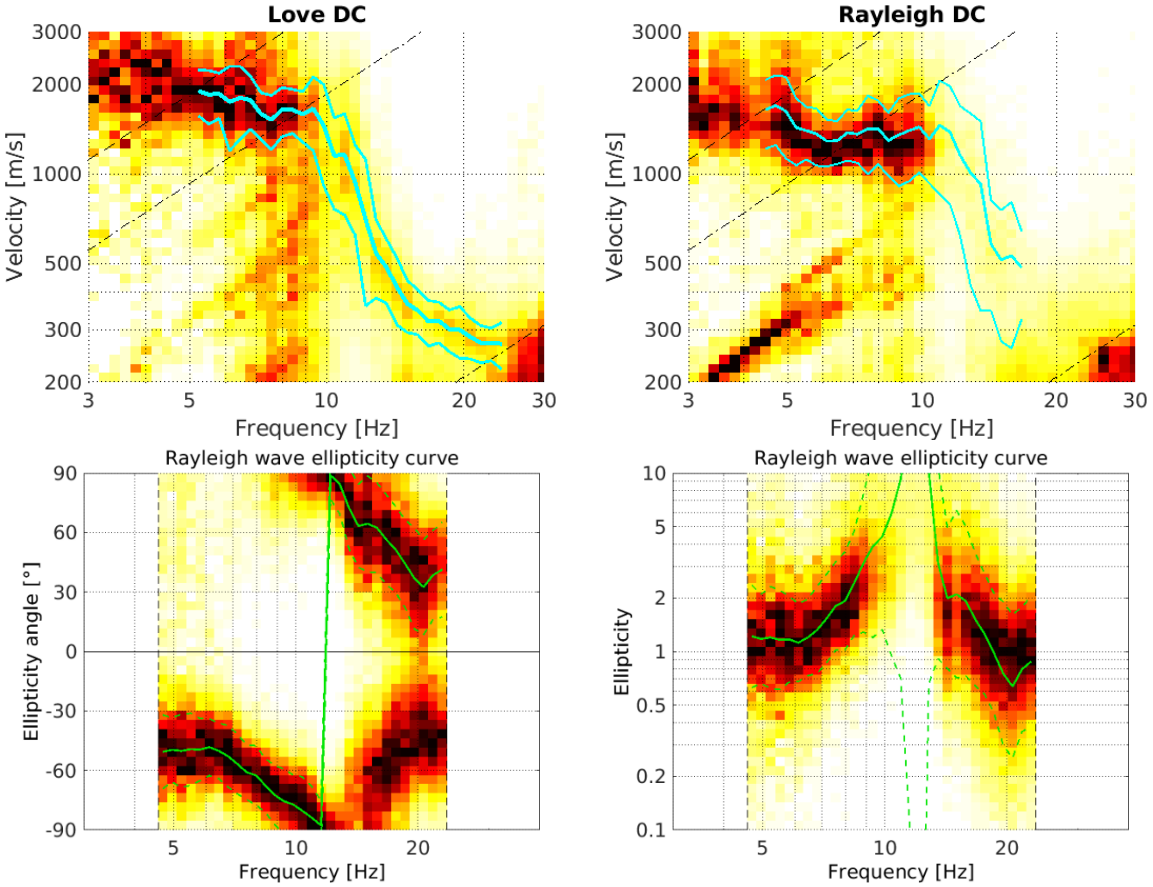

Figure 8: Dispersion and ellipticity curves for the Love and the Rayleigh waves obtained with WaveDec (Maranò et al., 2012). The solid cyan lines are picked from the data, where the central line indicates the best value and the two outer lines the standard deviation for the fundamental and first higher mode, respectively.

3.6 Summary

Figure 9 gives an overview of the dispersion and ellipticity curves determined by the different methods. For Love waves, WaveDec gives a dispersion curve that is similar to HRFK, but with slightly lower phase velocities. It is unclear if the HRFK curve corresponds to the same mode as the WaveDec curve or if it is rather the first higher mode.
For the Rayleigh waves, there is a good agreement between the WaveDec and vertical HRFK curves in the frequency range 4.0-10.0 Hz, but the higher mode is not clearly observed in WaveDec. The radial HRFK curve is not compatible with the vertical HRFK curve. The radial branch might actually correspond to the first higher mode below 12.0 Hz and to the fundamental mode above. In that case, the first higher mode could be continued by the second branch of the vertical HRFK.
The ellipticity curves retrieved using the different methods are quite different. The RayDec curve has a peak at about 11.0 Hz and the WaveDec curve defined for both ascendant and descendant flanks of the fundamental frequency peak gives higher values than the RayDec curve. The ellipticity retrieved from the HRFK radial component has the same shape as the RayDec curve, but the fundamental peak is shifted to higher frequency at about 14.0 Hz. This is in agreement with the dipping interface hypothesis in the area. Finally, the ellipticity obtained from the vertical component HRFK has a tendency to slightly increase its amplitude from 3.5 to about 10.0 Hz.
From the ellipticity angle is possible to observe the change of particle motion from retrograde to prograde at about 11.0 Hz (Fig. 8).

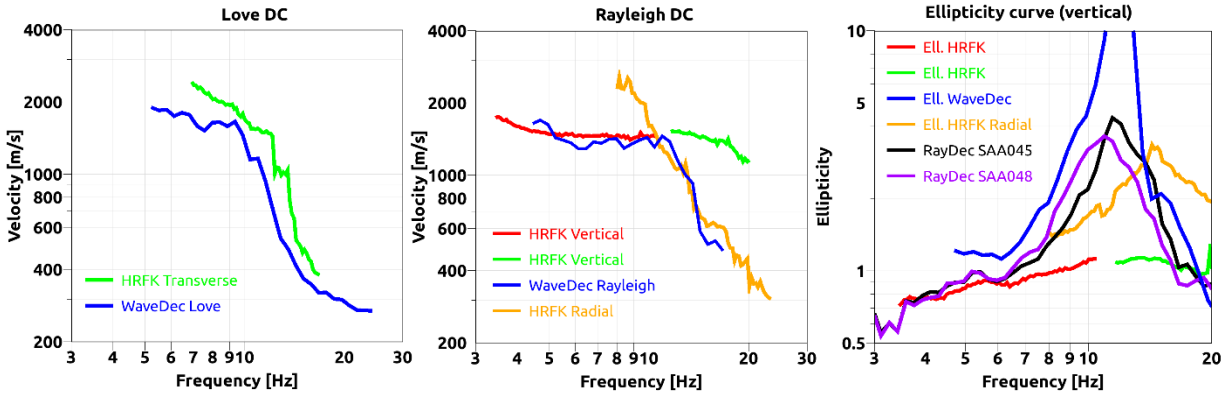

Figure 9: Comparison between the computed dispersion and ellipticity curves. The RayDec curve is related to the measurement point SAA045, whereas SAA048 is the closest to the seismic station.

4 Data inversion

4.1 Inversion targets

We performed inversions using as much information as possible from the different parts of the picked dispersion and ellipticity curves. The details of these inversion targets are indicated in Table 1 and the corresponding curves are shown in Fig. 10.
In the inversion process the WaveDec Love wave dispersion curve was used as the fundamental mode. For the Rayleigh wave dispersion curve, the vertical HRFK curve below 10.4 Hz and the radial HRFK curve above 11.6 Hz were used as fundamental mode. The second branch of the vertical HRFK was used as first higher mode.
In a first round of the inversion process, the RayDec ellipticity was also used, but we were unable to find velocity profiles explaining all the observed curves adding this information. The variability of the Löss thickness below the array measurement area could affect the ellipticity peak frequency extracted from different techniques (Fig. 9). Moreover, the RayDec peak could not be related to the fundamental mode, but to the first higher mode. Therefore, in the second inversion round, ellipticity was excluded.

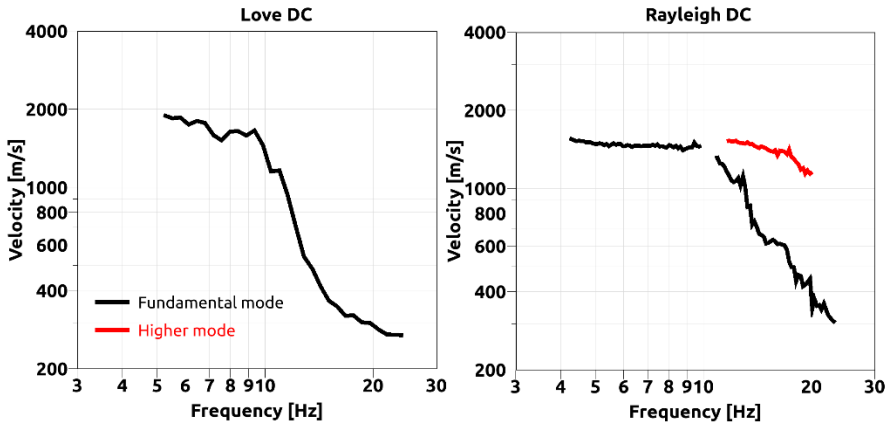

Figure 10: Overview of the dispersion curves used as targets for the different inversions.

Table 1: List of the data curves used as target in the inversion.

Method	Wave type	Mode	Curve type	Frequency range [Hz]
WaveDec	Love	fundamental	dispersion	5.2-24.2
HRFK (V)	Rayleigh	fundamental	dispersion	3.4-10.4
HRFK (V)	Rayleigh	first	dispersion	10.8-23.3
HRFK (R)	Rayleigh	fundamental	dispersion	11.6-20.1

4.2 Inversion parameterization

For the inversion, six different parameterizations are used in total. The first five have free values of the depths and velocities of the different layers, ranging from four to eight layers (including half-space). The last parameterization has fixed layer depths and consists of 15 layers in total, with the deepest interface at 40m depth.
The S- and P-wave velocities are allowed to range from 100 to 2500 m/s and from 200 to 5000 m/s, respectively. The deepest layer interfaces were allowed to range to a depth of 50 m for all parameterizations. The density was fixed to 2300 kg/m^3 for the bedrock layer and to 2000 kg/m^3 for all other layers.

4.3 Inversion results

We performed a total of six inversions with different parameterizations (see Table 2). Each inversion run produced 200000 total models in order to assure a good convergence of the solution. The results of these inversions are shown in Figs 11 – 16.

Table 2: List of inversions

Inversion	Number of layers	Number of models	Minimum misfit
SAARA4l	4	200000	0.4370
SAARA5l	5	200000	0.4454
SAARA6l	6	200000	0.4544
SAARA7l	7	200000	0.4629
SAARA8l	8	200000	0.4718
SAARAfix	15	200000	0.4761

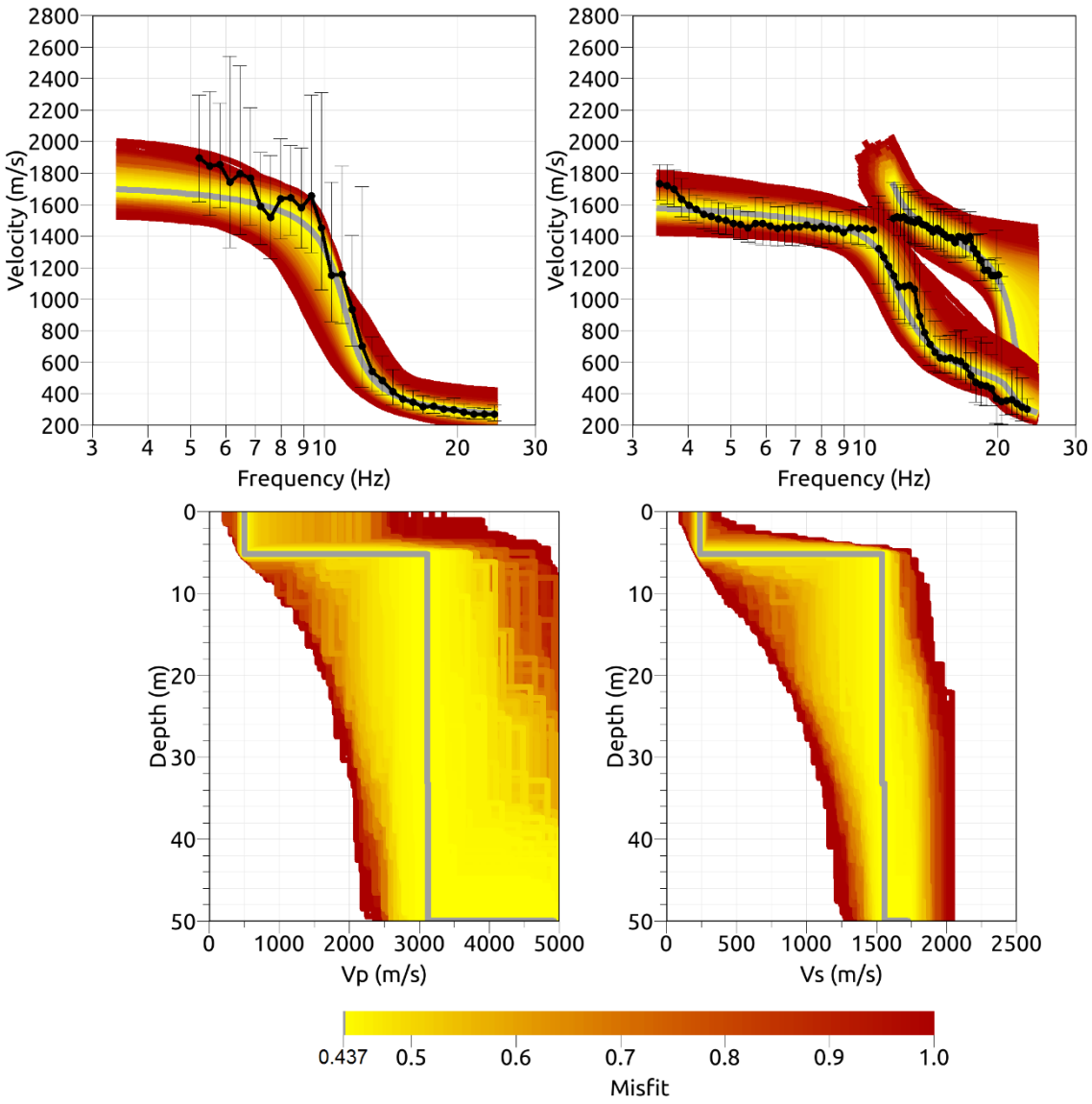

Figure 11: Inversion SAARA4l. Top line: Dispersion curves for the Love wave fundamental mode (left) and the Rayleigh wave fundamental and first higher mode (right). Bottom line: P-wave velocity profiles (left) and S-wave velocity profiles (right). The black dots indicate the data points used for the inversion, the gray line indicates the best-fitting model.

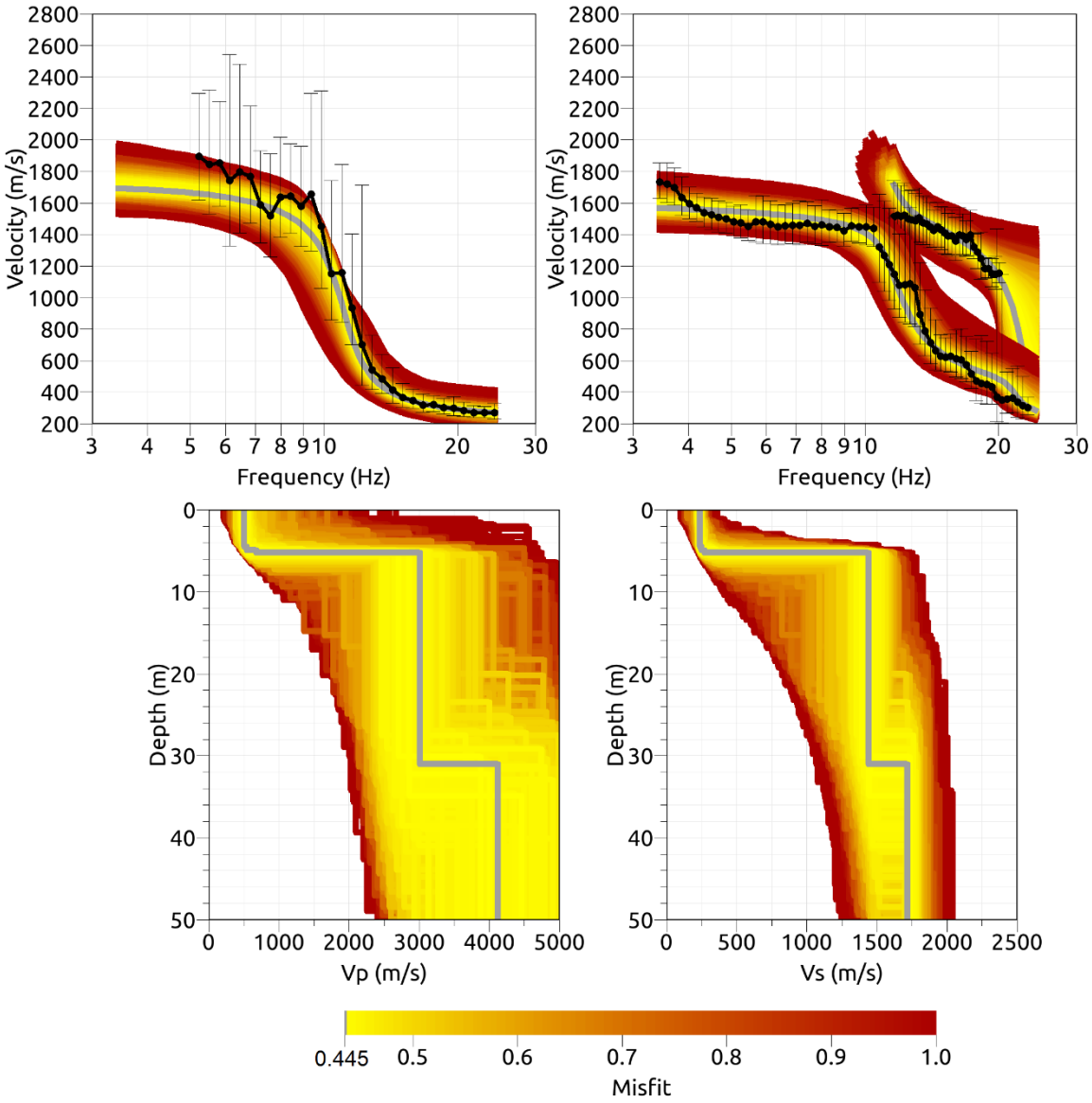

Figure 12: Inversion SAARA5l. Top line: Dispersion curves for the Love wave fundamental mode (left) and the Rayleigh wave fundamental and first higher mode (right). Bottom line: P-wave velocity profiles (left) and S-wave velocity profiles (right). The black dots indicate the data points used for the inversion, the gray line indicates the best-fitting model.

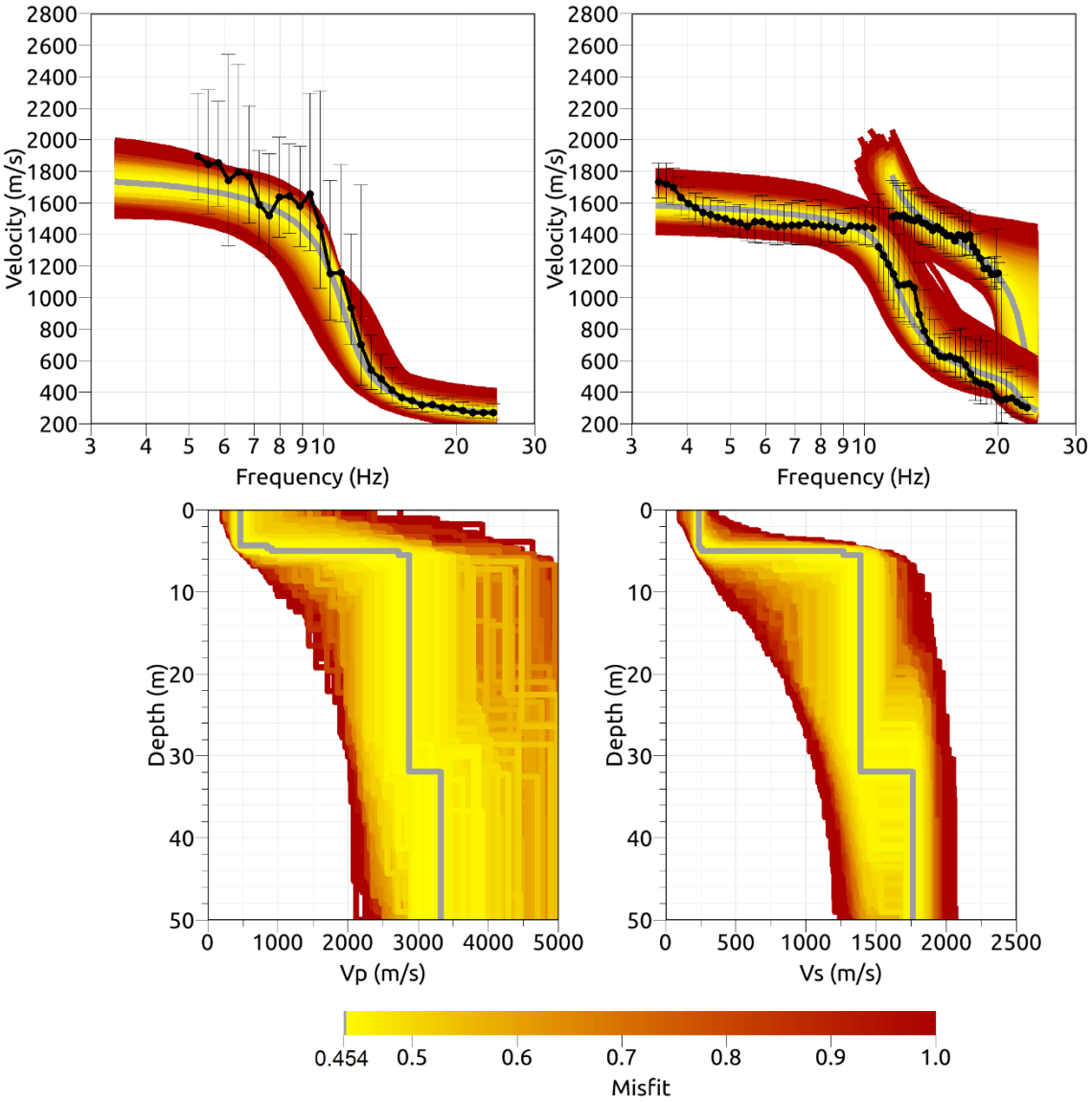

Figure 13: Inversion SAARA6l. Top line: Dispersion curves for the Love wave fundamental mode (left) and the Rayleigh wave fundamental and first higher mode (right). Bottom line: P-wave velocity profiles (left) and S-wave velocity profiles (right). The black dots indicate the data points used for the inversion, the gray line indicates the best-fitting model.

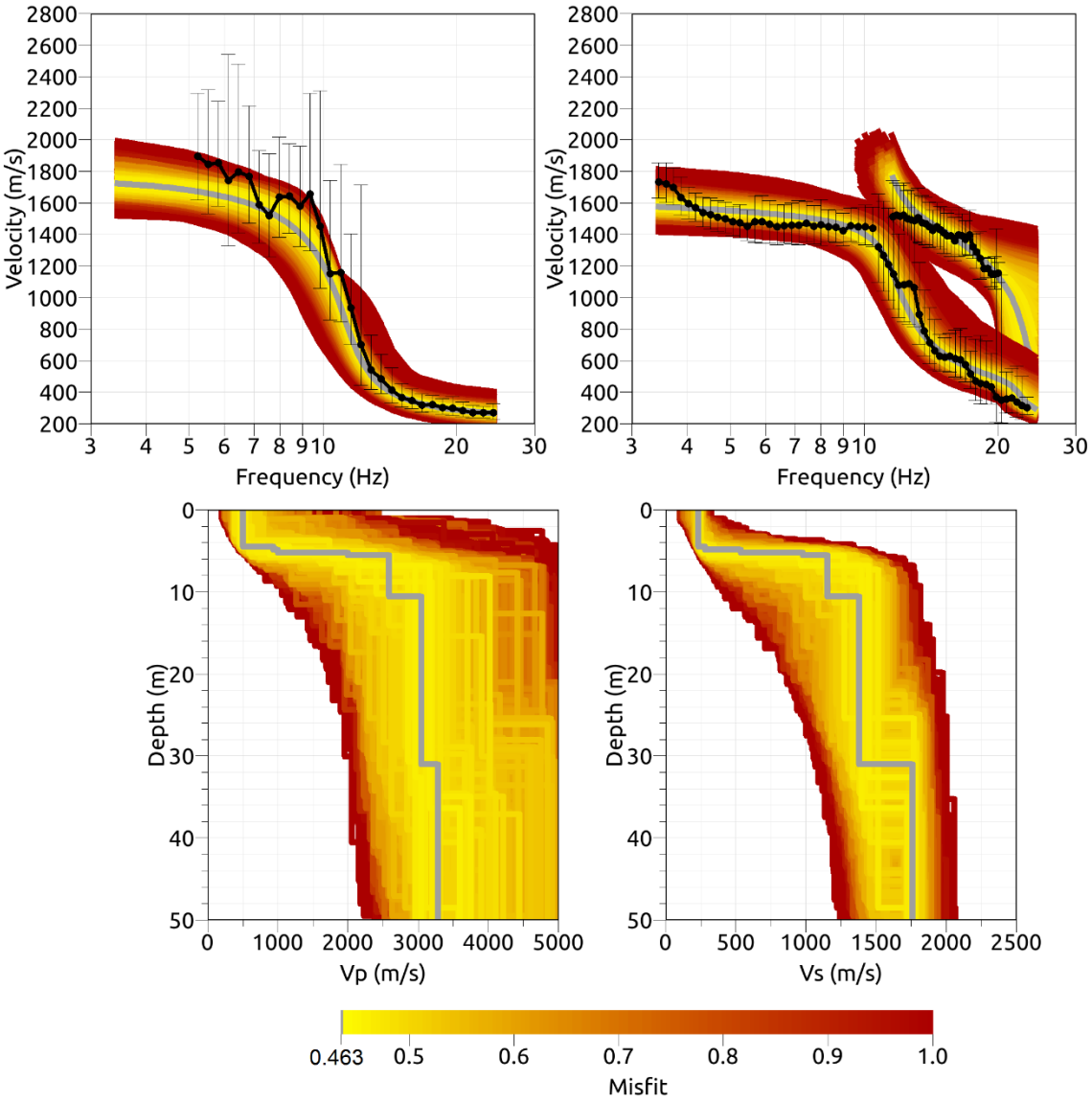

Figure 14: Inversion SAARA7l. Top line: Dispersion curves for the Love wave fundamental mode (left) and the Rayleigh wave fundamental and first higher mode (right). Bottom line: P-wave velocity profiles (left) and S-wave velocity profiles (right). The black dots indicate the data points used for the inversion, the gray line indicates the best-fitting model.

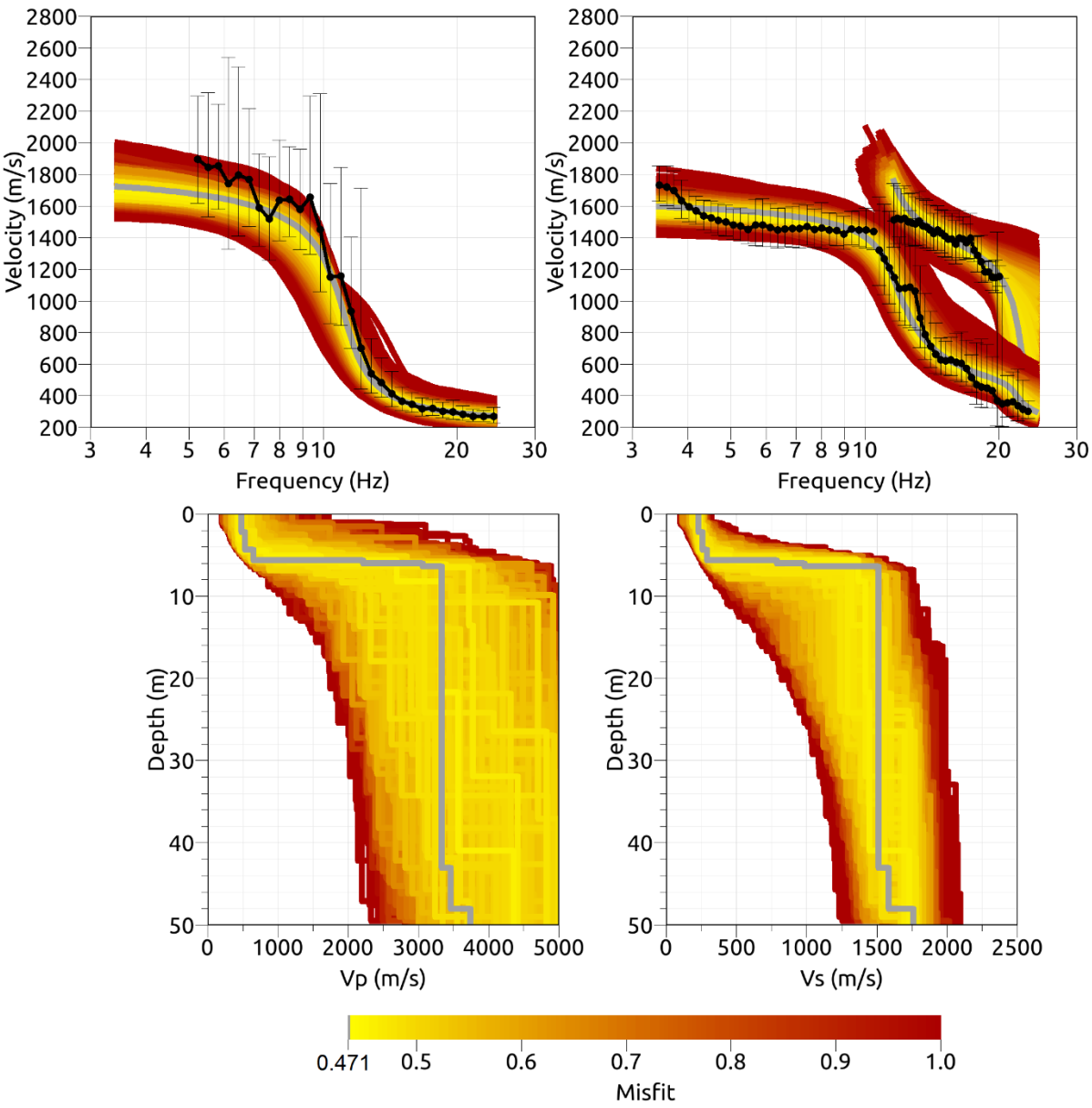

Figure 15: Inversion SAARA8l. Top line: Dispersion curves for the Love wave fundamental mode (left) and the Rayleigh wave fundamental and first higher mode (right). Bottom line: P-wave velocity profiles (left) and S-wave velocity profiles (right). The black dots indicate the data points used for the inversion, the gray line indicates the best-fitting model.

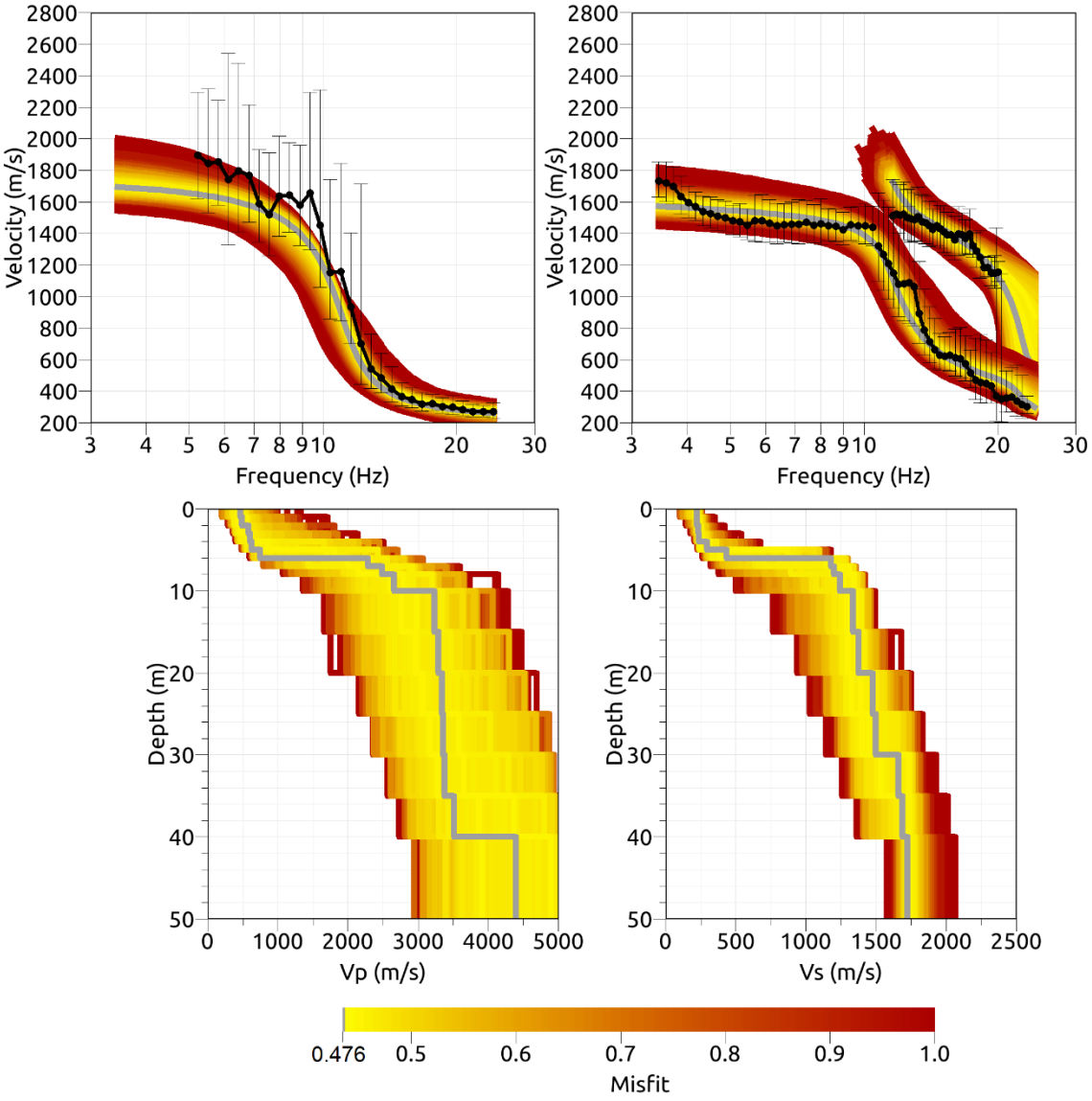

Figure 16: Inversion SAARAfix. Top line: Dispersion curves for the Love wave fundamental mode (left) and the Rayleigh wave fundamental and first higher mode (right). Bottom line: P-wave velocity profiles (left) and S-wave velocity profiles (right). The black dots indicate the data points used for the inversion, the gray line indicates the best-fitting model.

4.4 Discussion of the inversion results

The best-fitting models of the inversions are shown in Fig. 17. There are several main characteristics that all models have in common. The seismic bedrock is found at depths between 5.0 and 6.0 m, with a shear wave velocity of about 1600 m/s. Above the bedrock, the S-wave velocity is about 250.0 m/s. The velocity profiles resulting from the different inversions have V_{S30} between 740.8 and 796.9 m/s, with an average value of 765.7 ± 20.1 m/s.

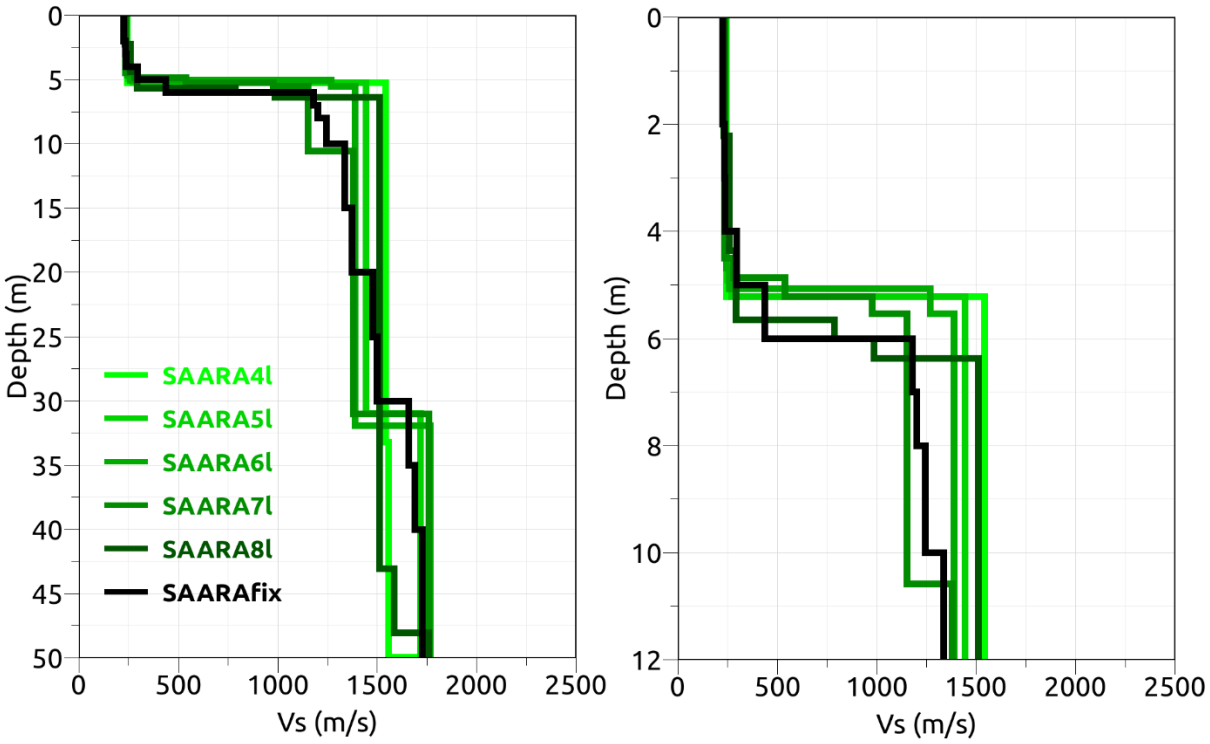

Figure 17: Overview of the shear-wave velocity profiles of the different inversions (left) and zoom on the upper 12 m of the inversion profiles.

5 Further results from the inverted profiles

5.1 SH transfer function

In Figure 18, the theoretical shear-wave transfer functions for the inverted models are shown. In this case, the models are predicting an amplification up to a factor of 5 at about 10.0 Hz. This is compared to observations of earthquake recordings at this station. The present empirical amplification function is not stable considering the low number of earthquakes used for its computation. As soon as the station has recorded a sufficiently large number of earthquakes the comparison will be made again.

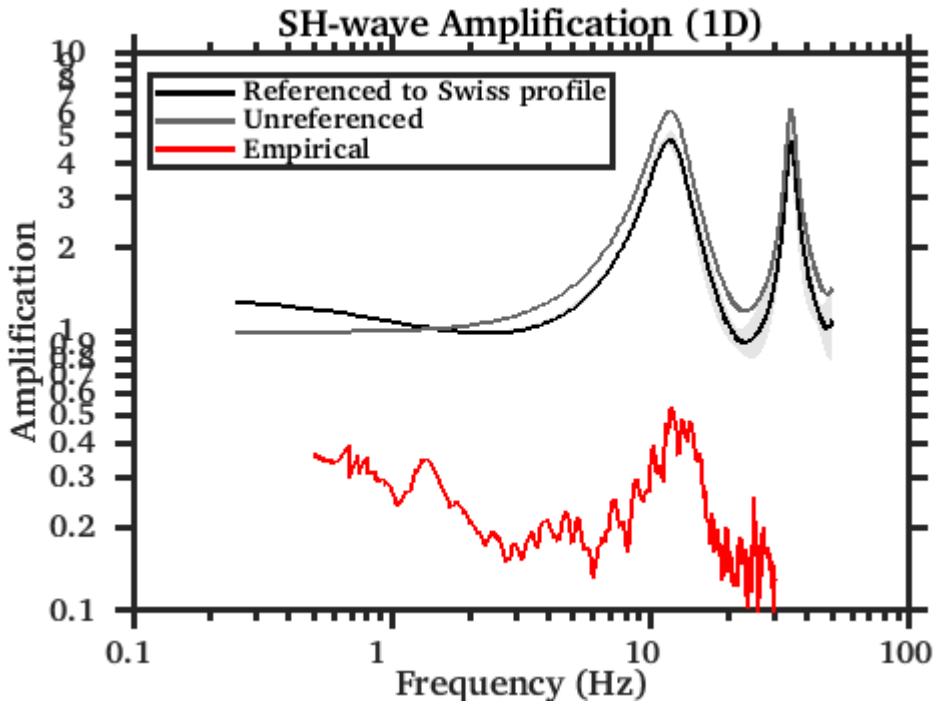

Figure 18: Modeled amplification function for the best models of the six inversions.

5.2 Quarter-wavelength representation

The quarter-wavelength velocity approach (Joyner et al., 1981) provides, for a given frequency, the average velocity at a depth corresponding to 1/4 of the wavelength of interest (Fig. 19). The results using this proxy, considering frequency limits of the experimental data of 3.5 to 25.0 Hz for the dispersion curves, is well constrained above 30 m. The quarter wavelength impedance-contrast introduced by Poggi et al. (2012) is also displayed in the figure. It corresponds to the ratio between two quarter-wavelength average velocities, respectively from the top and the bottom part of the velocity profile, at a given frequency.

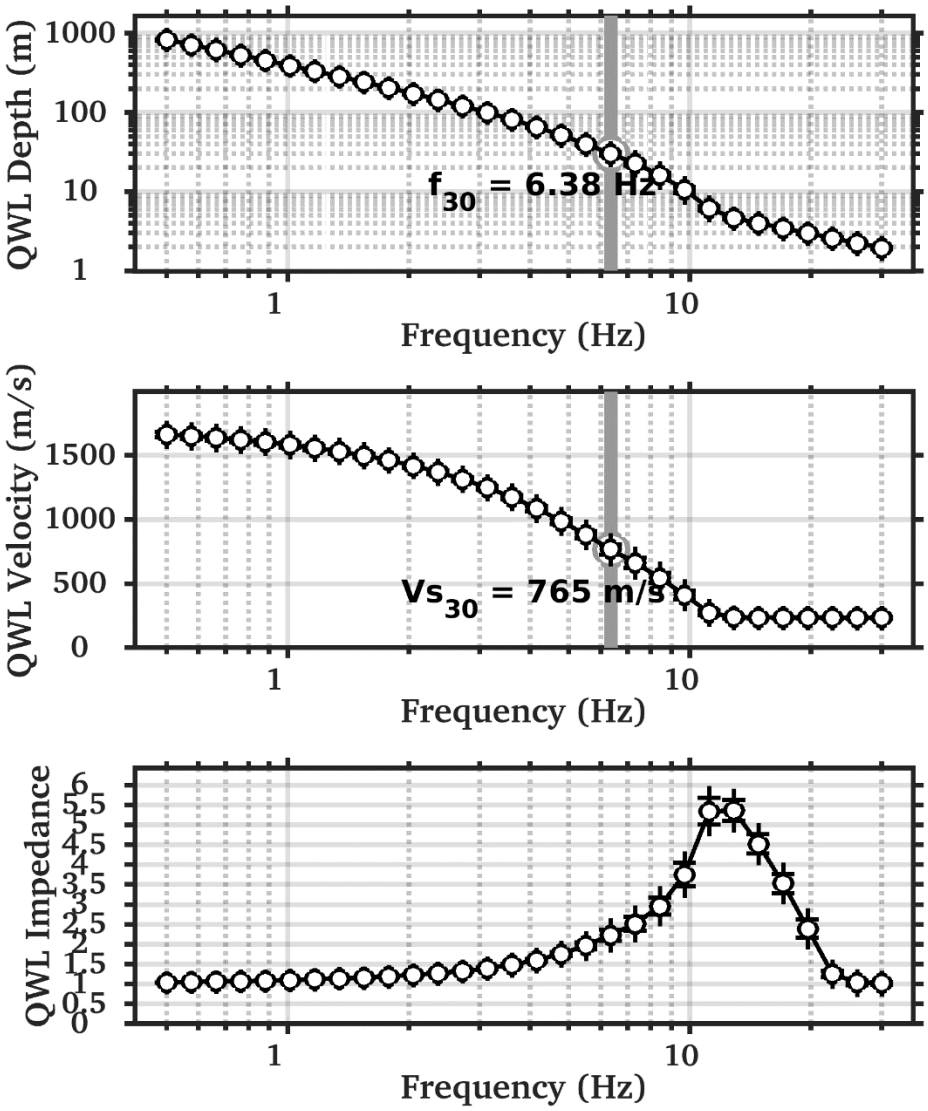

Figure 19: Quarter wavelength representation of the velocity profiles for the best models of the inversions (top: depth, center: velocity, bottom: inverse of the impedance contrast). The grey bar corresponds to f_{30} (frequency related to the of 30 m) and V_{S30}.

6 Discussion and conclusions

The H/V analysis points out that the fundamental peak observed at the different stations is variable and can be explained by a bedrock which is slightly dipping towards south.
The inversion of the passive seismic array measurements yields a velocity profile with a main interface at about 5-6 m. In particular, the soft layer has a velocity of about 250 m/s and the bedrock has a velocity of about 1600 m/s. The V_{S30} value of the site is about 765 m/s, corresponding to soil class B in EC8 and E in SIA261 classifications.
The theoretical shear-wave transfer function predicts an amplification factor of around 5 at about 10.0 Hz, in quite good agreement with the 10.9 Hz fundamental frequency of the site where the strong motion station is installed. This will be compared to observations at this station in the future.

Acknowledgements

The authors thank Anastasiia Shynkarenko for her help during the measurements.

References

Burjánek, J., Gassner-Stamm, G., Poggi, V., Moore, J. R., and Fäh, D. (2010). Ambient vibration analysis of an unstable mountain slope. Geophys. J. Int., 180:820–828.

Burjánek, J., Moore, J. R., Molina, F. X. Y., and Fäh, D. (2012). Instrumental evidence of normal mode rock slope vibration. Geophys. J. Int., 188:559–569.

Fäh, D., Gardini, D., et al. (2003). Earthquake Cataloque of Switzerland (ECOS) and the related macroseismic database. Eclogae geol. Helv. 96.

Fäh, D., Wathelet, M., Kristekova, M., Havenith, H., Endrun, B., Stamm, G., Poggi, V., Burjanek, J., and Cornou, C. (2009). Using ellipticity information for site characterisation. NERIES deliverable JRA4 D4, available at http://www.neries-eu.org.

Fritsche, S., Fäh, D., Gisler, M., and Giardini, D. (2006). Reconstructing the damage field of the 1855 earthquake inSwitzerland: historical investigations on a well-documented event Geophys. J. Int. (2006)166,719–731

Hobiger, M., Bard, P.-Y., Cornou, C., and Le Bihan, N. (2009). Single station determination of Rayleigh wave ellipticity by using the random decrement technique (RayDec). Geophys. Res. Lett., 36.

Maranò, S., Reller, C., Loeliger, H.-A., and Fäh, D. (2012). Seismic waves estimation and wavefield decomposition: Application to ambient vibrations. Geophys. J. Int., 191:175–188.

Poggi, V. and Fäh, D. (2010). Estimating Rayleigh wave particle motion from three component array analysis of ambient vibrations. Geophys. J. Int., 180:251–267.

Poggi, V., Edwards, B., and Fäh, D. (2010). Characterizing the Vertical-to-Horizontal Ratio of Ground Motion at Soft-Sediment Sites. Bulletin of the Seismological Society of America, 102(6): 2741 2756.